Supporting Information for

A Numerical Study of Lithospheric Deformation and Strain Partitioning Across the Longmen Shan Orogenic Belt, Eastern Tibetan Plateau

Yujun Sun *, Hailong Li, Taoyuan Fan

Chinese Academy of Geological Sciences, Beijing, 100037, China

* Corresponding author: Yujun Sun (sunyujunabc@163.com)

Contents of this file

This supporting information contains supply figures and tables presented and discussed in the text, and the numerical modeling data. Table S1 shows the rheological parameters of all cases. Figure S1 to S11 show the supply figures discussed in the text. Tables R1-R14 show the cumulative strain (the second invariant of the deviatoric strain tensor), strain rate (the second invariant of the deviatoric strain rate tensor), stress (the second invariant of the deviatoric stress tensor), temperature, and vertical heat flow for different cases in the text.

Additional supporting information

Table S1

Figures S1 to S11

Modeling data

Table R1-R14

Introduction

Description for Table S1

(1) Rheological parameters for two groups of models (Table S1).

Description for Figures S1 to S11:

(1) Distribution of the effective viscosity at different depth in the eastern Tibetan Plateau (Figure. S1);

(2) Distribution of the strength at different depth in the eastern Tibetan Plateau (Figure. S2);

(3) Distribution of the calculated stress (the second invariant of the deviatoric stress) for the different cases A (a), A1 (b), and A2 (c) (Figure. S3);

(4) Distribution of the calculated stress (the second invariant of the deviatoric stress) for the different cases B (a), B1 (b), and B2 (c) (Figure. S4);

(5) Predicted cumulative strain and strain rate for the different cases B2, B2-1, and B2-2. This figure shows the effects of the crustal strength of the Longmen Shan on lithospheric deformation and strain partitioning (Figure. S5);

(6) Comparison of the calculated topography (a), surface heat flow (b) with the observations for cases B2, B2-1, and B2-2 (Figure. S6);

(7) Predicted cumulative strain and strain rate for the different cases B3, B3-1, and B3-2. This figure shows the effects of the initial width of the Longmen Shan on lithospheric deformation and strain partitioning (Figure. S7).

(8) Comparison of the calculated topography (a), surface heat flow (b) with the observations for cases B3, B3-1, and B3-2 (Figure. S8).

(9) Predicted cumulative strain and strain rate for the different cases A1, A1-1, and A1-2. This figure shows the effects of the convergence velocity on lithospheric deformation and strain partitioning (Figure. S9).

(10) Predicted cumulative strain and strain rate for the different cases A3, A3-1, and A3-2. This figure shows the effects of the lower crustal viscosity in the Songpan-Ganzi terrane and Longmen Shan on lithospheric deformation and strain partitioning (Figure. S10).

(11) Comparison of the calculated topography (a), surface heat flow (b) with the observations for cases A3, A3-1, and A3-2 (Figure. S11).

Description for Table R1-R14

There are 150,000 markers used in the numerical model. Thus, we show the cumulative strain, strain rate, stress, temperature and vertical heat flow for every marker at different time steps. For each table at specific time, there are 150,000 rows and 5 columns. 150,000 rows present 150,000 markers at present time step.

The column 1 to column 7 follows:

Column 1: the x axis position (unit: meter. horizontal direction) for each marker at present time step.

Column 2: the y axis position (unit: meter. vertical direction) for each marker at present time step.

Column 3: the cumulative strain (the second invariant of the deviatoric strain ε_{II}) for each marker from 0 to present time step.

Column 4: the strain rate (the second invariant of the deviatoric strain rate $\dot{\varepsilon}_{II}$, unit: s^{-1}) for each marker at present time step.

Column 5: the stress (the second invariant of the deviatoric stress σ_{II}, unit: Pa) for each marker at present time step.

Column 6: the temperature (unit: ℃) for each marker at present time step.

Column 7: the vertical heat flow (unit: mW/m^2) for each marker at present time step.

Table R1: " caseA1_ 20Myr.csv" contains the cumulative strain, strain rate, stress, temperature and vertical heat flow after 20 Million years of convergence in case A1.

Table R2: " caseA2_ 20Myr. csv " contains the cumulative strain, strain rate, stress, temperature and vertical heat flow after 20 Million years of convergence in case A2.

Table R3: " caseA3_ 20Myr. csv " contains the cumulative strain, strain rate, stress, temperature and vertical heat flow after 20 Million years of convergence in case A3.

Table R4: " caseB1_ 20Myr. csv " contains the cumulative strain, strain rate, stress, temperature and vertical heat flow after 20 Million years of convergence in case B1.

Table R5: " caseB2_ 20Myr. csv " contains the cumulative strain, strain rate, stress, temperature and vertical heat flow after 20 Million years of convergence in case B2.

Table R6: " caseB3_ 20Myr. csv " contains the cumulative strain, strain rate, stress,

temperature and vertical heat flow after 20 Million years of convergence in case B3.
Table R7: " caseB21_ 20Myr. csv " contains the cumulative strain, strain rate, stress, temperature and vertical heat flow after 20 Million years of convergence in case B2-1. The upper and middle crustal strength of the Longmen Shan in this case is 50 MPa.
Table R8: " caseB22_ 20Myr. csv " contains the cumulative strain, strain rate, stress, temperature and vertical heat flow after 20 Million years of convergence in case B2-2. The upper and middle crustal strength of the Longmen Shan in this case is 10 MPa.
Table R9: " caseB31_20Myr. csv " contains the cumulative strain, strain rate, stress, temperature and vertical heat flow after 20 Million years of convergence based on case B3-1. The initial width of the Longmen Shan in this case is 100 km.
Table R10: " caseB32_20Myr. csv " contains the cumulative strain, strain rate, stress, temperature and vertical heat flow after 20 Million years of convergence based on case B3-2. The initial width of the Longmen Shan in this case is 50 km.
Table R11: " caseA11_ 26.7Myr.csv" contains the cumulative strain, strain rate, stress, temperature and vertical heat flow after 26.7 Million years of convergence in case A1-1. The velocity boundary imposed on the left boundary of the model in this case was 30 mm/yr.
Table R12: " caseA12_ 40Myr.csv" contains the cumulative strain, strain rate, stress, temperature and vertical heat flow after 40 Million years of convergence in case A1-2. The velocity boundary imposed on the left boundary of the model in this case was 40 mm/yr.
Table R13: " caseA31_ 20Myr. csv " contains the cumulative strain, strain rate, stress, temperature and vertical heat flow after 20 Million years of convergence in case A3-1. The viscosity imposed on the lower crust of the Songpan-Ganzi terrane and Longmen Shan was 1.0×10^{20} Pa · s in this case.
Table R14: " caseA32_ 20Myr. csv " contains the cumulative strain, strain rate, stress, temperature and vertical heat flow after 20 Million years of convergence in case A3-2. The viscosity imposed on the lower crust of the Songpan-Ganzi terrane and Longmen Shan was 5.0×10^{19} Pa · s in this case.

Table S1 Rheological parameters in two groups of models *.

Group A models							
Models	Layers	Songpan-Ganzi		Longmen Shan		Sichuan Basin	
		Viscosity (Pa • s)	Yield strength	Viscosity (Pa • s)	Yield strength	Viscosity	Yield strength
Case A1	Upper crust	1×10^{23}	10	1×10^{23}	10	5×10^{23}	100
	Middle crust	5×10^{22}	50	5×10^{22}	50	5×10^{23}	100
	Lower crust	5×10^{22}	50	5×10^{22}	50	5×10^{23}	100
	Mantle lithosphere	5×10^{22}	50	5×10^{22}	50	5×10^{23}	100
Case A2	Upper crust	1×10^{23}	10	1×10^{23}	10	5×10^{23}	20
	Middle crust	5×10^{22}	50	5×10^{22}	50	5×10^{23}	100
	Lower crust	5×10^{22}	50	5×10^{22}	50	5×10^{23}	100
	Mantle lithosphere	5×10^{22}	50	5×10^{22}	50	5×10^{23}	100
Case A3	Upper crust	1×10^{23}	10	1×10^{23}	10	5×10^{23}	20
	Middle crust	5×10^{22}	50	5×10^{22}	50	5×10^{23}	100
	Lower crust	1×10^{21}	50	1×10^{21}	50	5×10^{23}	100
	Mantle lithosphere	5×10^{22}	50	5×10^{22}	50	5×10^{23}	100

Group B models							
Models	Layers	Songpan-Ganzi		Longmen Shan		Sichuan Basin	
		Viscosity (Pa.s)	Yield strength	Viscosity (Pa.s)	Yield strength	Viscosity (Pa.s)	Yield strength
Case B1	Upper crust	1×10^{23}	10	1×10^{23}	100	5×10^{23}	100
	Middle crust	5×10^{22}	50	1×10^{23}	100	5×10^{23}	100
	Lower crust	5×10^{22}	50	5×10^{22}	50	5×10^{23}	100
	Mantle lithosphere	5×10^{22}	50	5×10^{22}	50	5×10^{23}	100
Case B2	Upper crust	1×10^{23}	10	1×10^{23}	100	5×10^{23}	100
	Middle crust	5×10^{22}	50	1×10^{23}	100	5×10^{23}	100
	Lower crust	1×10^{21}	50	1×10^{21}	50	5×10^{23}	100
	Mantle lithosphere	5×10^{22}	50	5×10^{22}	50	5×10^{23}	100
Case B3	Upper crust	1×10^{23}	10	1×10^{23}	100	5×10^{23}	10
	Middle crust	5×10^{22}	50	1×10^{23}	100	5×10^{23}	100
	Lower crust	1×10^{21}	50	1×10^{21}	50	5×10^{23}	100
	Mantle lithosphere	5×10^{22}	50	5×10^{22}	50	5×10^{23}	100

* Constant density was used in the model: 2600 kg/m^3 for the upper crust, 2800 kg/m^3 for the middle crust, 3000 kg/m^3 for the lower crust, and 3300 kg/m^3 for the mantle. Radioactive heat production of $Q_r^{upper\ crust} = 1.28 \times 10^{-6}\ W/m^3$, $Q_r^{middle\ crust} = 1.0 \times 10^{-6}\ W/m^3$ and $Q_r^{lower\ crust} = 0.8 \times 10^{-6}\ W/m^3$ were imposed on the upper crust, middle crust, and lower crust, respectively. Radioactive heat production for the mantle is 0. Thermal conductivities of $k^{upper\ crust} = 3.0\ \mathrm{W/(m \cdot K)}$, $k^{middle\ crust} = 3.0\ \mathrm{W/(m \cdot K)}$, $k^{lower\ crust} = 3.2\ \mathrm{W/(m \cdot K)}$, $k^{mantle\ lithosphere} = 3.4\ \mathrm{W/(m \cdot K)}$, $k^{asthenosphere} = 3.8\ \mathrm{W/(m \cdot K)}$ were imposed. Heat capacity $\mathrm{c} = 1300\ \mathrm{J/(kg \cdot K)}$ was used for all layers. The crust and mantle lithosphere have a visco-plastic rheology. The asthenosphere has viscous rheology, which does not include plastic deformation. The viscosity of the asthenosphere is 1×10^{21} Pa·s in all cases.

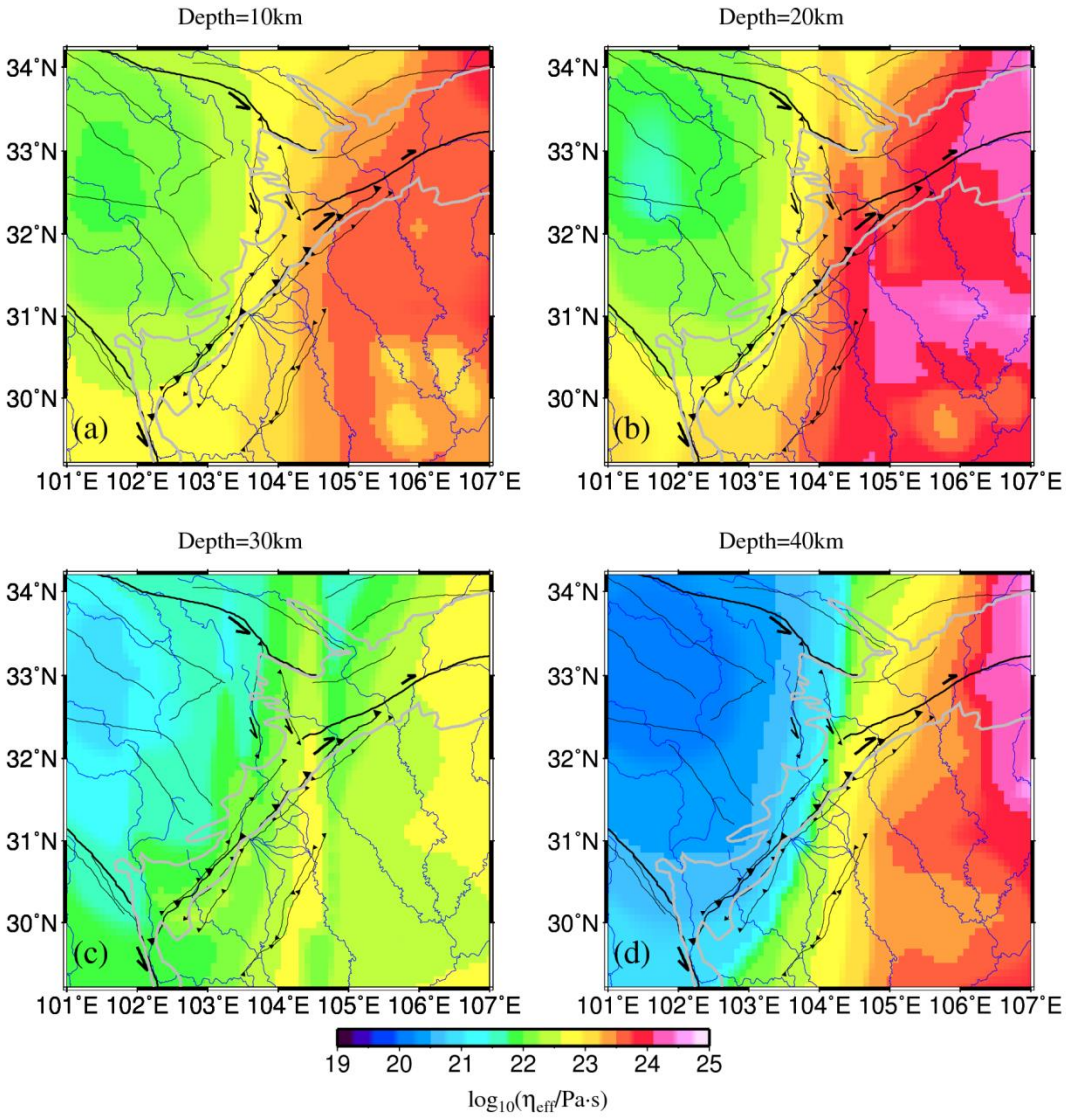

136

137 **Figure S1.** The calculated effective viscosity in this area (Sun et.al 2013a). Gray lines

138 indicate the Paleozoic/Proterozoic stratum (Figure 2), which are generally consistent

139 with the Longmen Shan orogenic belt. Black lines indicate the main faults in the study

140 area. Blue lines indicate the main rivers in this area.

141

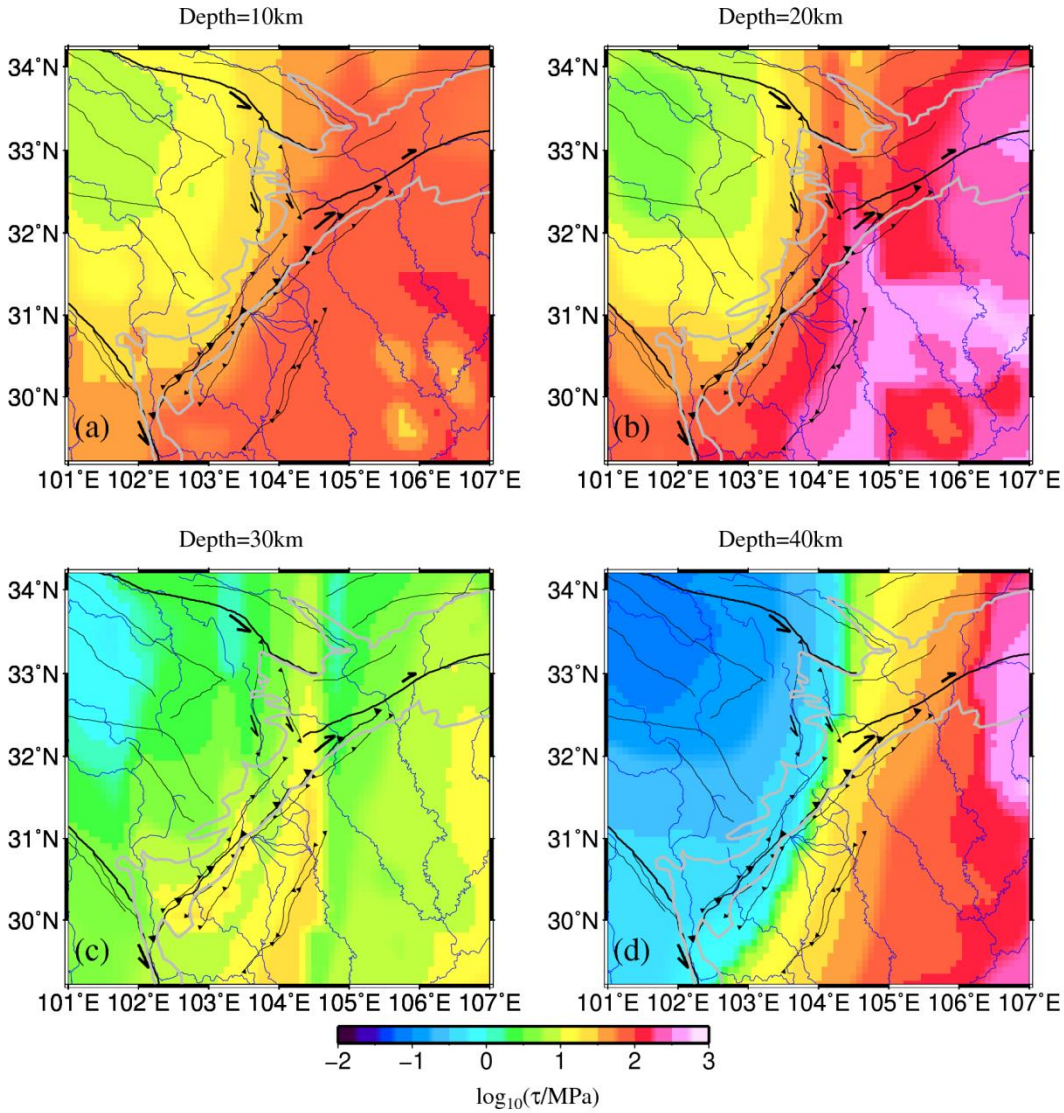

Figure S2. The calculated strength in this area (Sun et.al 2013a). Gray lines indicate the Paleozoic/Proterozoic stratum (Figure 2), which are generally consistent with the Longmen Shan orogenic belt. Black lines indicate the main faults in the study area. Blue lines indicate the main rivers in this area.

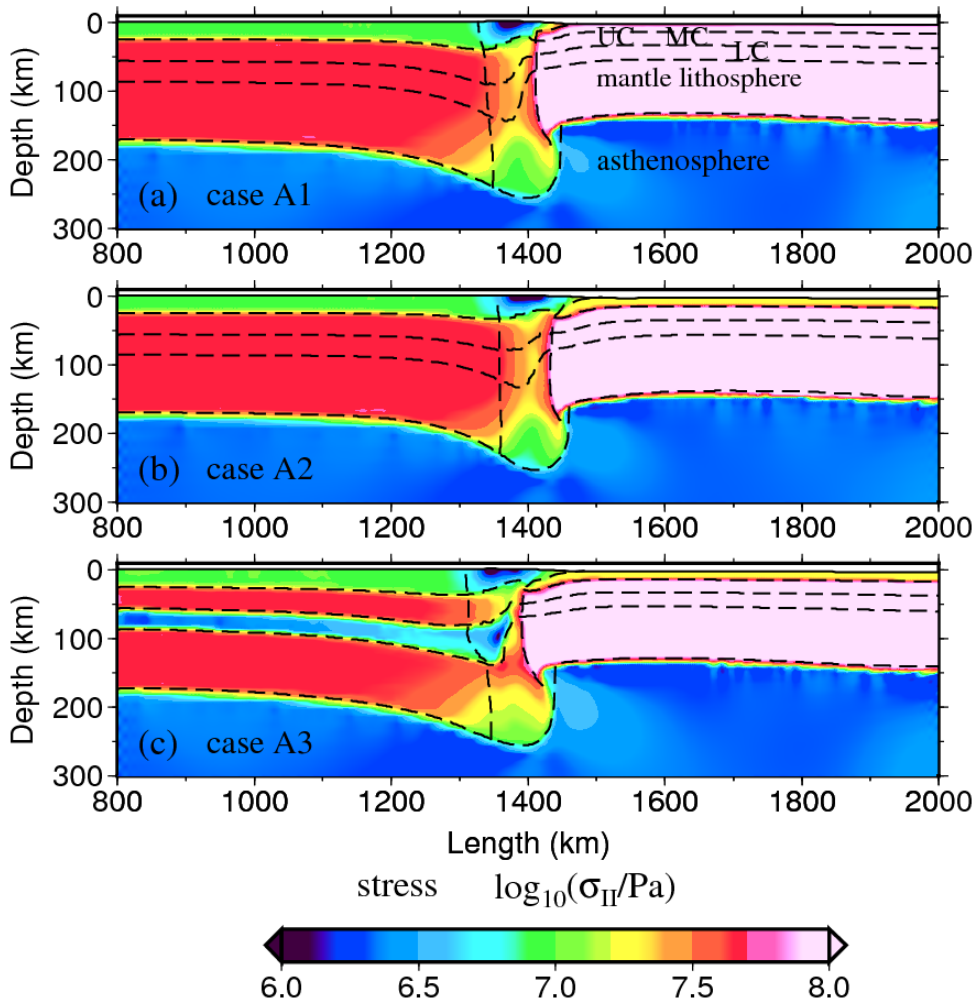

148

149 **Figure S3.** Distribution of the stress (the second invariant of the deviatoric stress

150 tensor) in the different cases (A1, A2, and A3) after 20 Myr of compression. Dashed

151 lines show the general boundaries of the different layers and blocks.

152

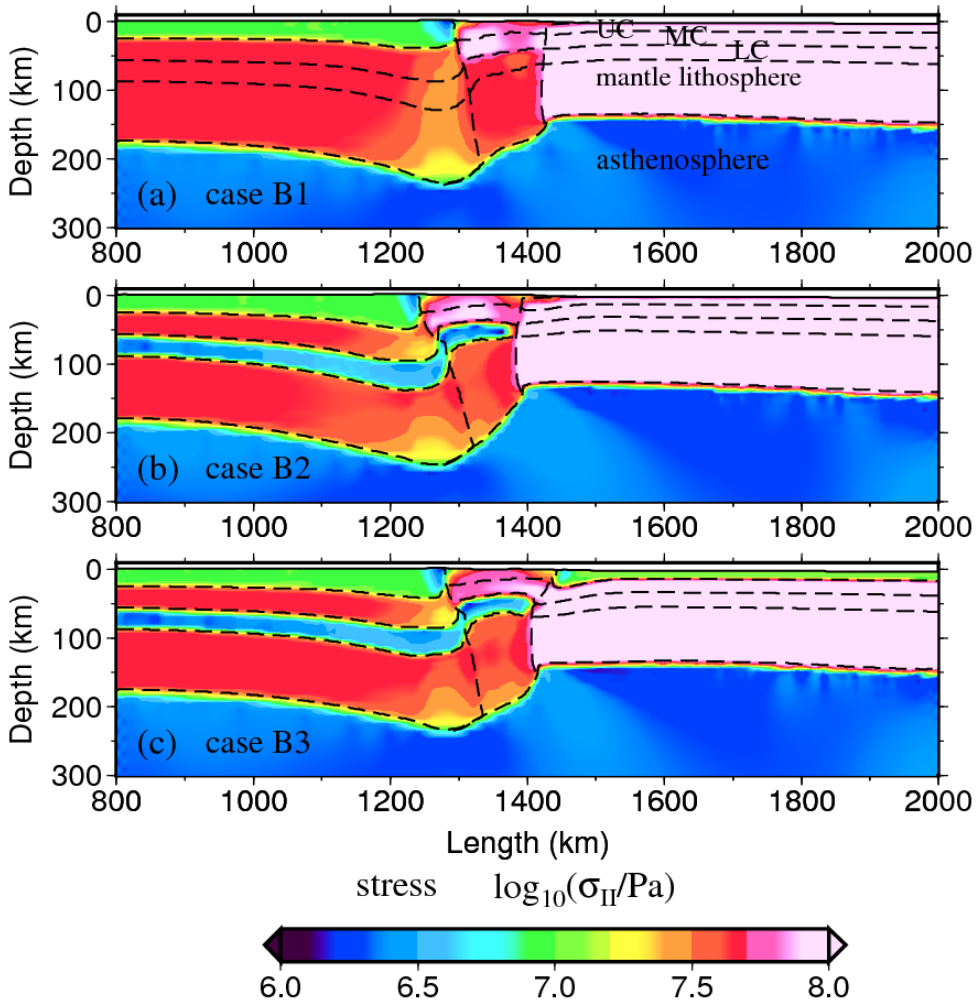

153

154 **Figure S4.** Distribution of the stress (the second invariant of the deviatoric stress

155 tensor) for the different cases (B1, B2, and B3) after 20 Myr of compression.

156

157

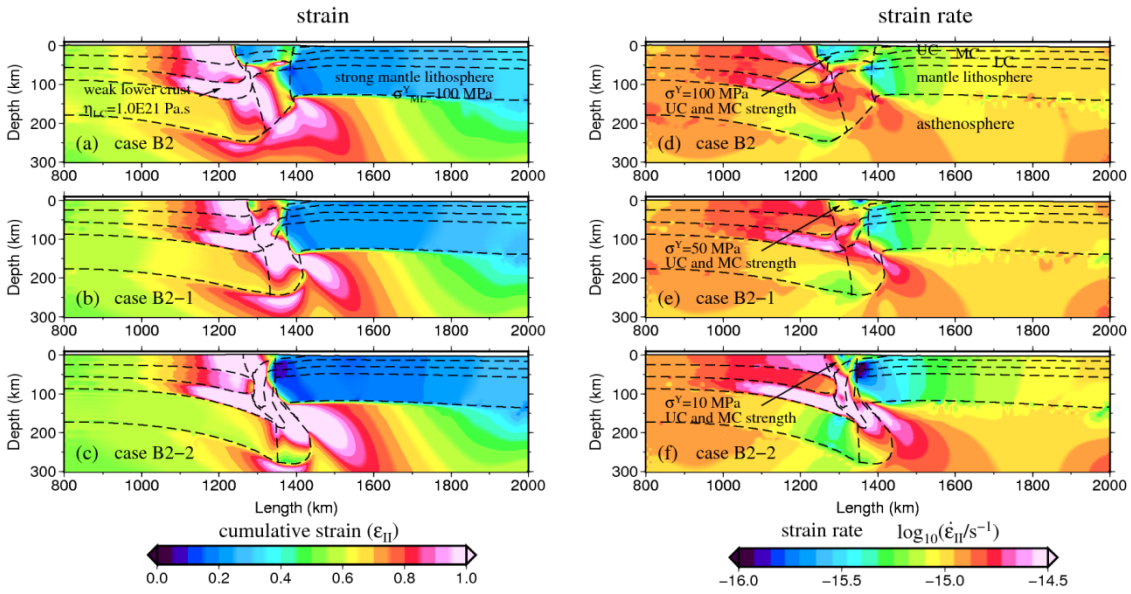

158

159 **Figure S5.** Effects of the crustal strength of the Longmen Shan on lithospheric

160 deformation and strain partitioning. Distribution of the cumulative strain (a-c) and

161 strain rate (d-f) in the different cases. The yield strength of the upper and middle crust

162 of the Longmen Shan is 100 MPa, 50 MPa, and 10 MPa in cases B2, B2-1, and B2-2,

163 respectively. The results of these cases are after 20 Myr of compression.

164

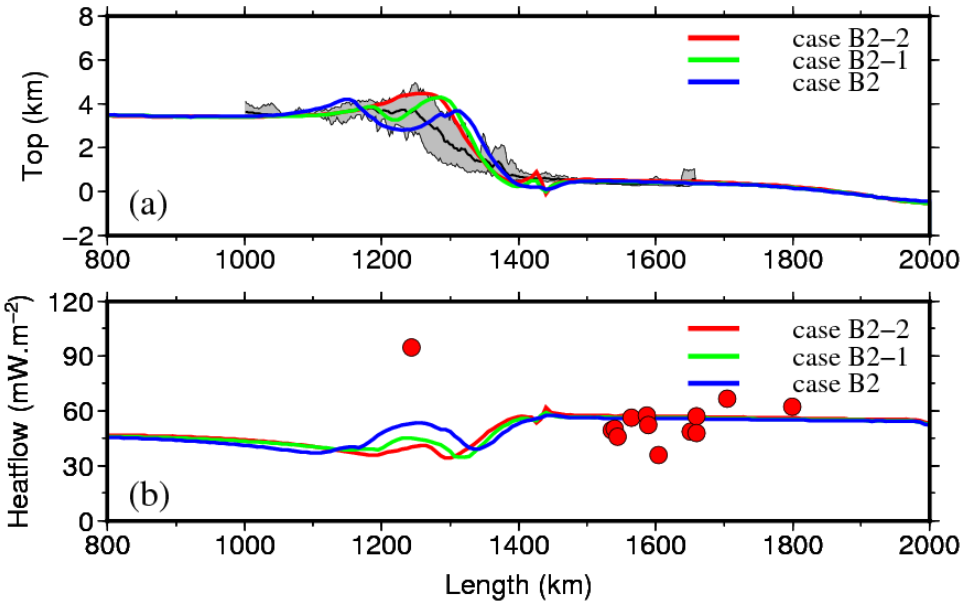

165

166 **Figure S6.** Comparisons of the predicted topography (a), and surface heat flow (b) of

167 the different cases (B2, B2-1, and B2-2) with the observations. Gray area (a) indicates

168 the topographic profile across the northern segment of the Longmen Shan. Red dots (b)

169 show the surface heat flow across this profile. These results are derived from different

170 cases after 15 Myr of compression.

171

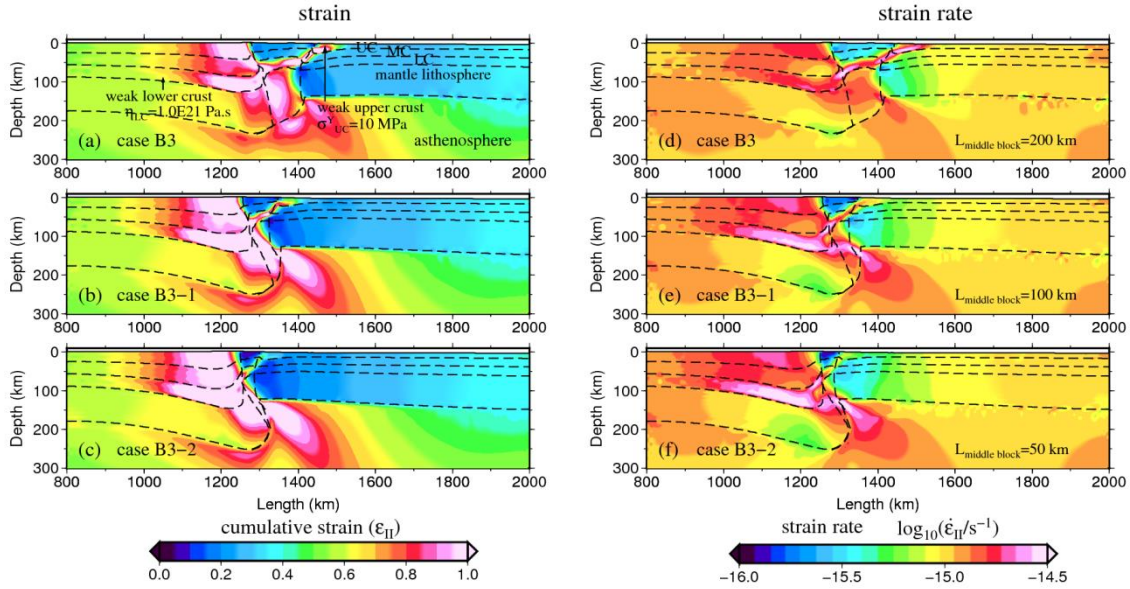

172

173 **Figure S7.** Effect of the scale of the Longmen Shan on lithospheric deformation and

174 strain partitioning. Distribution of the cumulative strain (a-c) and strain rate (d-f) in

175 the different cases. The initial length of the Longmen Shan is 200 km, 100 km and 50

176 km in cases B3, B3-1, and B3-2, respectively. The results of these cases are after 20

177 Myr of compression.

178

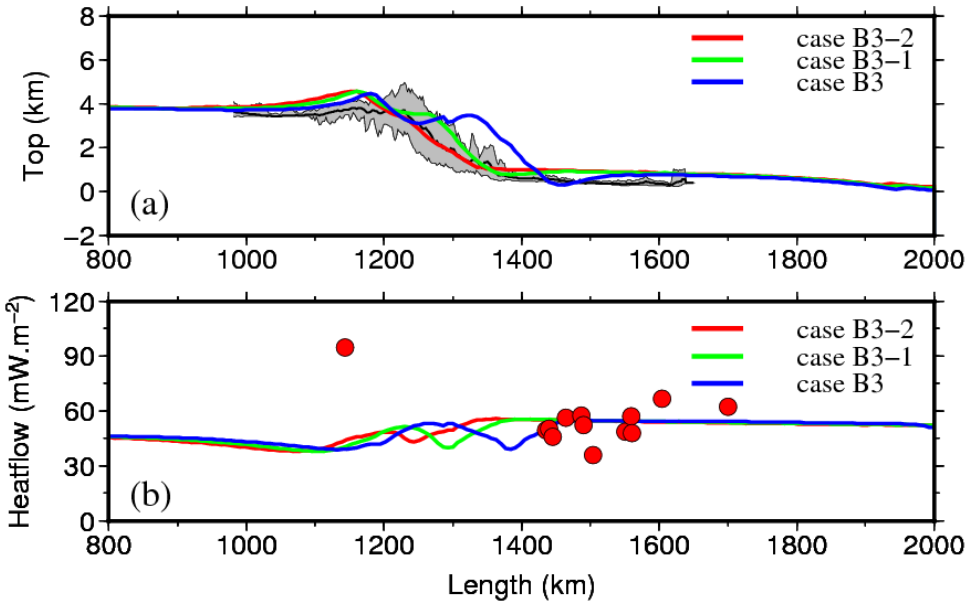

179

180 **Figure S8.** Comparison of the predicted topography (a), and surface heat flow (b) in

181 the different cases (B3, B3-1, and B3-2) with the observations. Gray area (a) indicates

182 the topographic profile across the northern segment of the Longmen Shan. Red dots (b)

183 show the surface heat flow across this profile. These results are derived from different

184 cases after 15 Myr of compression.

185

186

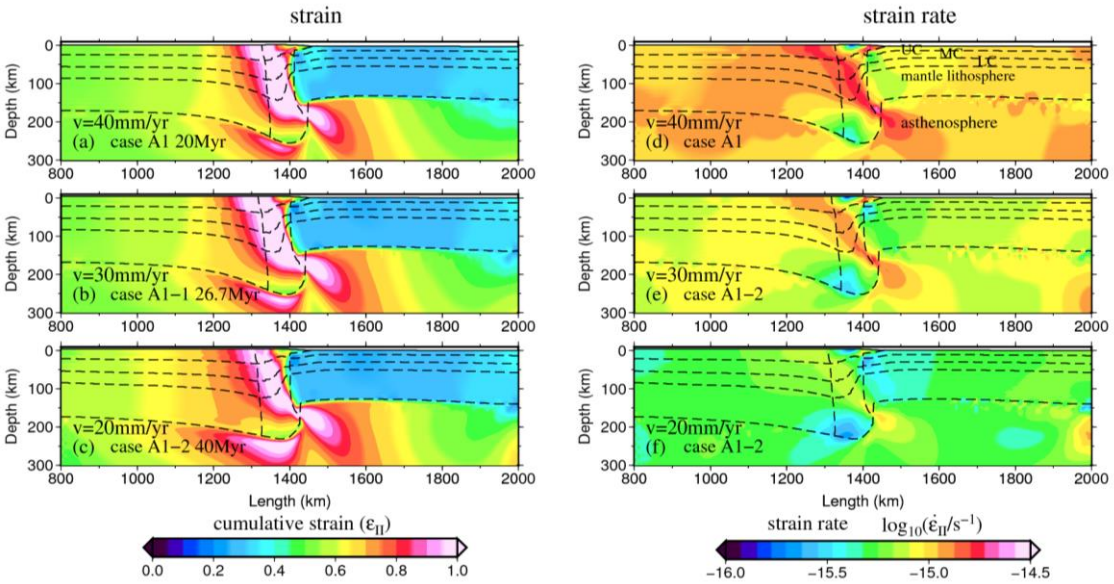

187

188 **Figure S9.** Effect of the velocity boundary condition on lithospheric deformation and
189 strain partitioning. Distribution of the cumulative strain (a-c) and strain rate (d-f) in
190 different cases. The velocities imposed on the left side of the model were 40 mm/yr,
191 30 mm/yr, and 20 mm/yr in cases A1, A1-1, and A1-2, respectively. The results shown
192 in this figure are 20 Myr (a, d), 26.7Myr (b, e), and 40 Myr (c, f) of compression,
193 respectively. So the same amount of convergence (800 km) was imposed.

194

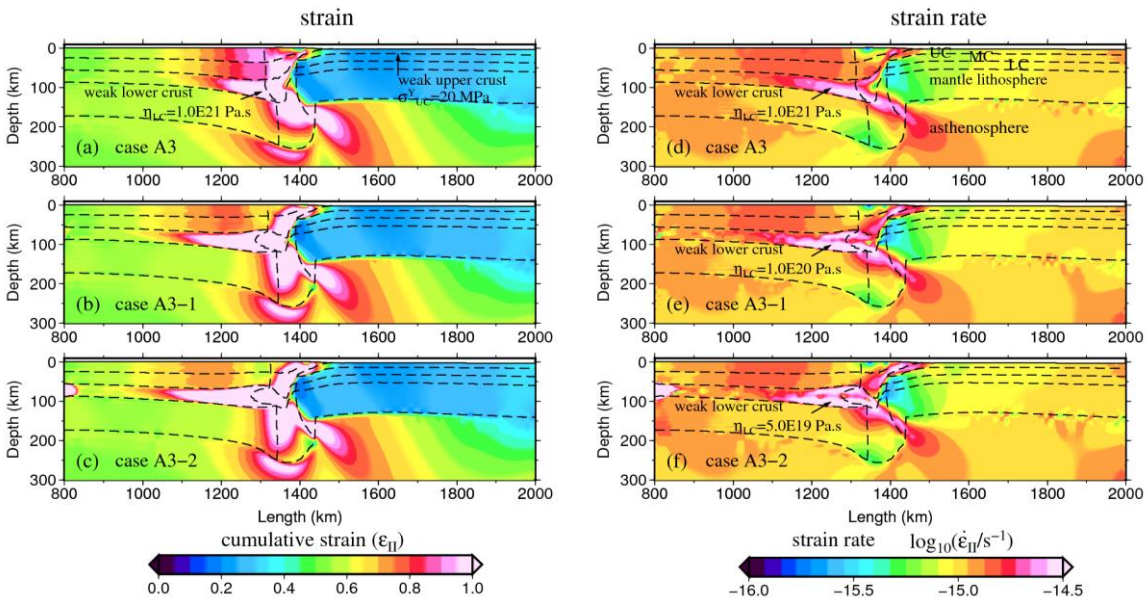

Figure S10. Effect of the lower crustal viscosity of the Songpan-Ganzi terrane on lithospheric deformation and strain partitioning. Distribution of the cumulative strain (a-c) and strain rate (d-f) for different cases. The viscosities imposed on the lower crust of the Songpan-Ganzi terrane and Longmen Shan were 1.0×10^{21} Pa · s, 1.0×10^{20} Pa · s, and 5.0×10^{19} Pa · s in cases A3, A3-1, and A3-2, respectively. respectively. The results shown in this figure are 20 Myr of compression.

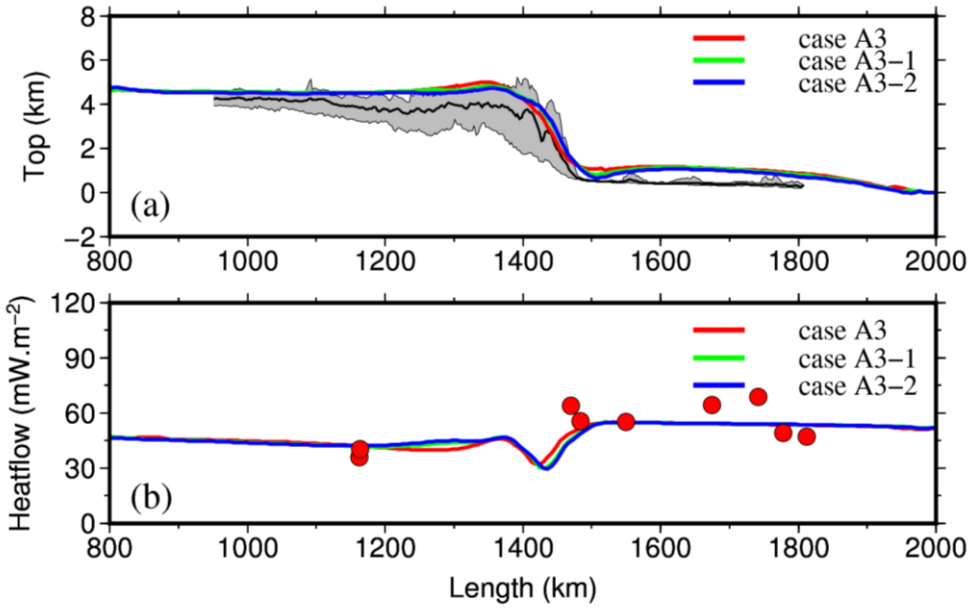

203

204 **Figure S11.** Effect of the lower crustal viscosity of the Songpan-Ganzi terrane on the

205 topography and surface heat flow in the different cases after 20 Myr of compression.

206